IOP Publishing Journal of Optics
J. Opt. **12** (2010) 124005 (9pp) doi:10.1088/2040-8978/12/12/124005

Singular optical reordering of liquid crystals using Gaussian beams

Etienne Brasselet

Centre de Physique Moléculaire Optique et Hertzienne, Université Bordeaux 1, CNRS, 33405 Talence Cedex, France

E-mail: e.brasselet@cpmoh.u-bordeaux1.fr

Received 2 February 2010, accepted for publication 13 April 2010
Published 11 November 2010
Online at stacks.iop.org/JOpt/12/124005

Abstract
We introduce the concept of singular optical reordering of birefringent elastic media using Gaussian beams. Theoretical and experimental results are reported in the particular case of a uniformly aligned nematic liquid crystal film illuminated at normal incidence by a circularly polarized beam. The longitudinal component of the light field is demonstrated to be at the origin of cylindrically symmetric singular reorientation of the optical axis that can be described by the superposition of a radial and azimuthal elastic distortion field. Moreover, the handedness of the overall reorientation pattern is controlled by the handedness of the incident beam circular polarization.

Keywords: optical reorientation, liquid crystals, singular patterning, longitudinal optical vortex

(Some figures in this article are in colour only in the electronic version)

1. Introduction

Liquid crystals can self-assemble into various phases characterized by well-defined orientational ordering of their crystalline axis and are well known to be sensitive to external fields. Light is no exception. Indeed the high birefringence and low elastic constants of liquid crystals confer to them genuinely high optical nonlinearities that are essentially driven by their orientational degree of freedom. Although these orientational optical nonlinearities can be triggered either by resonant or nonresonant light–matter interaction processes [1] here we will consider only the case of purely dielectric optical reorientation.

A famous example is the optical Fréedericksz transition experimentally demonstrated in nematic liquid crystals by Zolot'ko *et al* in 1981 [2], which is associated with the spectacular appearance of laser-induced diffraction rings [3]. The optical reordering of thermotropic liquid crystals, for which the temperature controls the successive appearance of distinct mesophases [4], has been the subject of long lasting research activities that were very productive in the 1980s [5]. In particular the self-induced stimulated light scattering phenomenon, where the Stokes shift is driven by the light itself, was unveiled [6, 7]. During the 1990s, significant advances were made by exploring various polarization states for the excitation light [8–11] and, more particularly, the transition from regular to chaotic reorientation dynamics was thoroughly investigated by many groups [12–15]. A renewed interest appeared during the last decade in the context of chaos [16–19] and also following the discovery of a secondary instability above the Fréedericksz transition under circularly polarized light [20]. This eventually led to an accurate theoretical description of laser-induced nonlinear dynamics in the plane wave limit [21–23]. Moreover, light–matter angular momentum exchanges were no longer restricted to spin angular momentum but extended to the orbital angular momentum as well [24, 25], for which a mature modeling toolbox is now available [26].

Until now, optical reordering of liquid crystals has been experimentally discussed, and theoretically described, in the framework of a smooth spatial reorientation profile (i.e., a spatial distribution of the molecular axes free from orientational singularities) generated by smooth optical fields (i.e., light beams free from optical singularities). The generation of singular orientational patterns in liquid crystals using Gaussian beams is nevertheless possible, as shown recently in [27]. Here our purpose is to introduce in more detail the concept of singular optical reordering of birefringent and elastic media.

The particular case of a uniformly aligned nematic liquid crystal film illuminated at normal incidence by a circularly

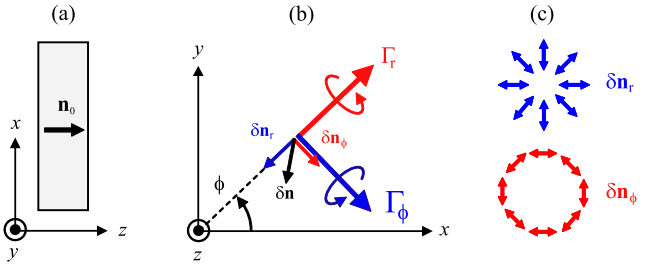

Figure 1. (a) Unperturbed homeotropic nematic liquid crystal film. (b) Radial ($\mathbf{\Gamma}_r$) and azimuthal ($\mathbf{\Gamma}_\phi$) components of the optical dielectric torque density that lead to azimuthal ($\delta\mathbf{n}_\phi$) and radial ($\delta\mathbf{n}_r$) elastic distortions, respectively. In this example $\Gamma_r > 0$ and $\Gamma_\phi < 0$, which leads to $\delta n_\phi < 0$ and $\delta n_r < 0$, respectively. (c) Sketch of the cylindrically symmetric radial and azimuthal reorientation modes.

polarized fundamental Gaussian beam is considered in this work. In fact, the longitudinal component of the light field is at the origin of a space-variant optical torque density that generates radial and azimuthal elastic distortions. Such laser-induced singular reorganization of the liquid crystal ordering is theoretically addressed in section 2, and experimental observations are reported in section 3.

2. Model

2.1. Qualitative considerations

Let us consider a non-magnetic dielectric material illuminated by a light field. Neglecting nonlinear electronic susceptibilities, the material acquires a polarization density $\mathbf{P}$, which is related to the electric field $\mathbf{E}$ by a linear tensorial relationship. As a result, an optical torque density $\mathbf{\Gamma}_{\rm light} = \frac{1}{2}\,{\rm Re}(\mathbf{P}^* \times \mathbf{E})$ is exerted on the medium (the complex notation is used). As a matter of fact $\mathbf{\Gamma}_{\rm light} \neq \mathbf{0}$ when the polarization and the electric field are not collinear, which can happen in anisotropic dielectrics such as liquid crystals. In the case of uniaxial nematics, the optical axis orientation is defined by a unit vector $\mathbf{n}$ called the director, which represents the local average orientation of the liquid crystal molecules, and $\mathbf{\Gamma}_{\rm light} = \frac{\epsilon_a}{8\pi}\,{\rm Re}[(\mathbf{n}\cdot\mathbf{E}^*)(\mathbf{n}\times\mathbf{E})]$ in Gaussian units, where $\epsilon_a = \epsilon_\parallel - \epsilon_\perp$ is the dielectric permittivity anisotropy and symbols ($\perp$, $\parallel$) refer to directions perpendicular and parallel to $\mathbf{n}$, respectively.

For the purpose of illustration, we choose a homogeneous nematic slab lying in the (x, y) plane that has its optical axis at rest, $\mathbf{n}_0$, along the z axis (see figure 1(a)). Therefore

$$\mathbf{\Gamma}_{\rm light} = \frac{\epsilon_a}{8\pi}\,{\rm Re}(-E_z^* E_\phi\,\mathbf{e}_r + E_z^* E_r, \mathbf{e}_\phi), \tag{1}$$

$$= \Gamma_r\,\mathbf{e}_r + \Gamma_\phi\,\mathbf{e}_\phi, \tag{2}$$

where $(\mathbf{e}_r, \mathbf{e}_\phi, \mathbf{e}_z)$ is the cylindrical coordinate system. Obviously, $\mathbf{\Gamma}_{\rm light} = 0$ for a plane wave since $E_z = 0$ in that case. A real light beam, however, can exert non-zero radial ($\mathbf{\Gamma}_r$) and azimuthal ($\mathbf{\Gamma}_\phi$) torque densities due to a non-zero longitudinal component for the light field. Consequently, azimuthal ($\delta\mathbf{n}_\phi$) and radial ($\delta\mathbf{n}_r$) elastic distortions of the unperturbed state $\mathbf{n}_0$ are expected from $\mathbf{\Gamma}_r$ and $\mathbf{\Gamma}_\phi$, respectively, as illustrated in figure 1(b).

The general expression for the perturbed director $\mathbf{n} = \mathbf{n}_0 + \delta\mathbf{n}$ is therefore written

$$\delta\mathbf{n} = \delta n_r\,\mathbf{e}_r + \delta n_\phi\,\mathbf{e}_\phi + \delta n_z\,\mathbf{e}_z, \tag{3}$$

where $\delta n_z = (1-\delta n_r^2 - \delta n_\phi^2)^{1/2} - 1$ (recall that $|\mathbf{n}| = 1$) and we introduce two cylindrically symmetric collective reorientation modes, which we will further refer to as the radial and the azimuthal modes, as illustrated in figure 1(c). Note that the excitation of these modes requires an optical torque density that does not depend on ϕ. This suggests the use of a circularly polarized fundamental Gaussian beam as the simplest choice in practice, which is retained here both for modeling and experimental purposes.

Readers who are familiar with the optical Fréedericksz transition problem might be surprised to read about optical reordering of nematics without a threshold. Indeed this looks in contradiction to the common statement that optical reorientation occurs above a threshold when a light beam is normally incident onto a homeotropic nematic film (i.e., perpendicular alignment). However, this is true only for the ideal case of a plane wave, where the optical torque density on the unperturbed state is zero. In contrast, our considerations hold for any real beam. In other words, the optical Fréedericksz transition problem in the real world implies singular optical reordering, at least for low light intensities, as demonstrated in this study. Obviously, this does not prevent spontaneous symmetry breaking and the transition to regular optical reordering at larger intensities, as discussed in section 3.3.

2.2. Quantitative description

The model is derived in a standard way from the minimization of the total free energy [5]

$$\mathcal{F} = \int_0^L \int_0^\infty \int_0^{2\pi} r\,(F_{\rm el} + F_{\rm opt})\,{\rm d}\phi\,{\rm d}r\,{\rm d}z, \tag{4}$$

where $F_{\rm el,opt}$ are the elastic and optical free energy densities, respectively. In addition, the input facet of the nematic film is located at $z = 0$ and L is the film thickness. Within the single elastic constant approximation

$$F_{\rm el} = \tfrac{1}{2}K[(\nabla\cdot\mathbf{n})^2 + |\nabla\times\mathbf{n}|^2], \tag{5}$$

where K is the Frank elastic constant and

$$F_{\rm opt} = -\frac{1}{16\pi}\epsilon_{ij}E_i E_j^*, \tag{6}$$

where $\{i, j\} = \{x, y, z\}$ and the dielectric permittivity tensor is

$$\epsilon_{ij} = \epsilon_\perp\delta_{ij} + \epsilon_a n_i n_j. \tag{7}$$

A basic requirement is the evaluation of the electric field inside the nematic, which is a complicated task when $\delta\mathbf{n} \neq \mathbf{0}$. However, by restricting the model to small distortion amplitude we retain the electric field expression that follows from its propagation on the unperturbed state $\mathbf{n} = \mathbf{n}_0$, thereby neglecting the feedback of optical reorientation on the light

field itself. This can be done according to the work of Ciattoni *et al* [28] that deals with the propagation of a circularly polarized Gaussian beam inside a c-cut uniaxial crystal in the paraxial approximation. In practice such an approach benefits from the simple expression for the transverse part of the field derived in [29] where the birefringence is considered as a small parameter. The longitudinal component is then obtained from the procedure detailed in [30]. We get, in the Cartesian coordinate system $(\mathbf{e}_x, \mathbf{e}_y, \mathbf{e}_z)$, up to the unimportant phase factor $\exp(-\mathrm{i}\omega t + \mathrm{i}k_0 n_\perp z \pm \mathrm{i}\phi)$ that will disappear once inserted in equation (6),

$$\mathbf{E}_\pm = \frac{E_0 G}{\sqrt{2}}\Big[(\mathrm{e}^{\mp\mathrm{i}\phi}\cos\Delta + \mathrm{i}\,\mathrm{e}^{\pm\mathrm{i}\phi}\sin\Delta)\,\mathbf{e}_x \pm \mathrm{i}(\mathrm{e}^{\mp\mathrm{i}\phi}\cos\Delta - \mathrm{i}\,\mathrm{e}^{\pm\mathrm{i}\phi}\sin\Delta)\,\mathbf{e}_y - \frac{r}{Z}\,\mathbf{e}_z\Big], \tag{8}$$

where the $\pm$ signs refer to left- and right-handed incident circular polarizations that are represented by the unit vectors $\mathbf{c}_\pm = (\mathbf{e}_x \pm \mathrm{i}\mathbf{e}_y)/\sqrt{2}$, respectively; $G = -(\mathrm{i}z_0/Z)\exp(\mathrm{i}\beta r^2/Z)$ is the spatial profile of the fundamental Gaussian beam, whose waist is located at $z = 0$, with $Z = z - \mathrm{i}z_0$, $\beta = \pi n/\lambda$, $z_0 = \pi n w_0^2/\lambda$ the Rayleigh distance, $n = (n_\perp + n_\parallel)/2$ and λ the wavelength; $k_0 = 2\pi/\lambda$; ω is the pulsation frequency; $\Delta = \varepsilon\beta r^2 z/Z^2$ with $\varepsilon = (n_\parallel - n_\perp)/n$ and $n_{\parallel,\perp} = \epsilon_{\parallel,\perp}^{1/2}$ the refractive indices along and perpendicular to $\mathbf{n}$, respectively.

Note that the Cartesian representation given by equation (8) can be put in a more compact form in the cylindrical coordinate system using $\mathbf{c}_\pm = (\mathbf{e}_\mathrm{r} \pm \mathrm{i}\mathbf{e}_\phi)\,\mathrm{e}^{\pm\mathrm{i}\phi}/\sqrt{2}$:

$$\mathbf{E}_\pm = \frac{E_0 G}{\sqrt{2}}\left(\mathrm{e}^{\mathrm{i}\Delta}\,\mathbf{e}_\mathrm{r} \pm \mathrm{e}^{-\mathrm{i}\Delta}\,\mathbf{e}_\phi - \frac{r}{Z}\,\mathbf{e}_z\right). \tag{9}$$

Once the optical field is known, a set of coupled partial differential Euler–Lagrange equations for $\delta\mathbf{n}_\mathrm{r}$ and $\delta\mathbf{n}_\phi$ can be obtained from the calculus of variations for $\mathcal{F}$. Instead, for the sake of simplicity, the distorted director field is sought by imposing an ansatz for the two independent radial and azimuthal modes. In this way, analytical expressions can be obtained.

First, note that a circularly polarized Gaussian beam leads to cylindrically symmetric radial and azimuthal torque densities since $\partial\Gamma_{\mathrm{r},\phi}/\partial\phi = 0$ (see equations (1) and (9)). Therefore $\partial\delta n_{\mathrm{r},\phi}/\partial\phi = 0$ and we will assume $\delta n_{\mathrm{r},\phi} = \mathcal{R}(r)\mathcal{Z}(z)$. The longitudinal boundary condition $\mathbf{n} = \mathbf{n}_0$ at $z = (0, L)$ gives $\mathcal{Z}(0) = \mathcal{Z}(L) = 0$, thus allowing the expansion of $\mathcal{Z}$ on the Fourier basis, $\mathcal{Z}(z) = \sum_m A^{(m)}\sin(mqz)$, where m are positive integers and $q = \pi/L$. On the other hand, the absence of reorientation far away from the beam imposes $\mathcal{R}(\infty) = 0$, whereas the cylindrical symmetry ensures $\mathcal{R}(0) = 0$. A physically acceptable radial dependence is then grasped by noting that the radial and azimuthal torque are both proportional to the longitudinal electric field component and quadratic in the electric field amplitude, see equation (1). Since $E_z \propto r$ and $E_{\mathrm{r},\phi,z} \propto G$, see equation (9), we thus retain a dependence on r of the form $\mathcal{R}(r) = (r/w)\exp(-2r^2/w^2)$, where w is a characteristic length. In summary, the radial and azimuthal distortion fields are sought in the form

$$\delta n_{\mathrm{r},\phi}(r, z) = \frac{r}{w_{\mathrm{r},\phi}}\exp(-2r^2/w_{\mathrm{r},\phi}^2)\sum_m A_{\mathrm{r},\phi}^{(m)}\sin(mqz), \tag{10}$$

where $A_{\mathrm{r},\phi}^{(m)}$ and $w_{\mathrm{r},\phi}$ refer to the mode amplitudes and waists, respectively. In what follows the longitudinal modal expansion is restricted to the first modes only ($m = 1$) in order to establish a minimal model.

The stationary reoriented state is then found by minimizing $\mathcal{F}$ with respect to the set of unknowns $\mathbf{u} = (A_\mathrm{r}^{(1)}, A_\phi^{(1)}, w_\mathrm{r}, w_\phi)$. This gives a system of four coupled equations:

$$\frac{\partial\mathcal{F}}{\partial u_k} = 0 \qquad \text{with } k = \{1, 2, 3, 4\}, \tag{11}$$

and, since there is no possible confusion when dealing with the monomodal approximation, the superscripts on the mode amplitudes will be further omitted. This system of equations is rewritten $\mathbf{S}(\mathbf{u}) = \mathbf{0}$, where $\mathbf{S}$ is given in appendix A and an approximate analytical solution is given in appendix B. The zeros of $\mathbf{S}$ are evaluated numerically using a Newton–Raphson method. In simulations we used $n_\perp = 1.53$ and $n_\parallel = 1.77$ for the refractive indices of the nematic liquid crystal E7 used in the experiments, and $L = 100\ \mu$m for the film thickness. Also, we introduced the longitudinal and transverse reduced lengths as multiples of the characteristic lengths z_0 and w_0, respectively: $\tilde{z} = z/z_0$, $\tilde{L} = L/z_0$, $\tilde{q} = qz_0$, $\tilde{r} = r/w_0$ and $\tilde{w}_{\mathrm{r},\phi} = w_{\mathrm{r},\phi}/w_0$. Finally, we defined the reduced power $\tilde{P} = P_0/P_\mathrm{c}$ with $P_0 = \frac{c}{8\pi}n|E_0|^2\int_0^{2\pi}\int_0^\infty r\exp(-2r^2/w_0^2)\,\mathrm{d}r\,\mathrm{d}\phi$ the total incident power and $P_\mathrm{c} = cK/n$ a characteristic power for the optical reorientation of the nematic, c being the speed of light in free space (P_c equals a few milliwatts for usual nematics).

From a general point of view, when the beam waist is located at $z = 0$, $A_\mathrm{r} < 0$ whereas the sign of the azimuthal mode amplitude depends on the incident beam polarization handedness, namely $A_\phi < 0$ ($A_\phi > 0$) in the $\mathbf{c}_+$ ($\mathbf{c}_-$) case. This can be qualitatively understood by noting that the optical torque density exerted onto the unperturbed director is expressed as $\mathbf{\Gamma}_\pm \propto \pm\mathbf{e}_\mathrm{r} - \tilde{z}\mathbf{e}_\phi$ in the limit of small birefringence. Consequently, $\Gamma_\phi < 0$ whatever the incident polarization handedness, hence $A_\mathrm{r} < 0$ as illustrated in figure 1(b). Moreover $\Gamma_\mathrm{r} > 0$ ($\Gamma_\mathrm{r} < 0$) for $\mathbf{c}_+$ ($\mathbf{c}_-$) incident polarization, hence $A_\phi < 0$ ($A_\phi > 0$), see figure 1(b). Typical radial and azimuthal patterns are shown in figures 2(a) and (b) and the influence of the polarization handedness of the pump light beam is demonstrated in figures 2(c) and (d) that emphasize the chiral character of the optically induced elastic distortion field.

The power dependence of $A_{\mathrm{r},\phi}$ is shown in figure 3(a) and the maximal distortion amplitude in the (x, y) plane, $|\delta\mathbf{n}_\perp|_\mathrm{max} = [\delta n_\mathrm{r}^2(r, z) + \delta n_\phi^2(r, z)]_{z=L/2}^{1/2}$, is displayed in figure 3(b). As expected from section 2.1, the singular optical reordering does not exhibit a threshold behavior. More quantitatively, the absolute value of the reorientation amplitude monotonously increases with power for both modes, whatever the beam waist. This is demonstrated in figure 3(a), where the cases $\tilde{L} = 10$ (red curves, label 1), $\tilde{L} = 1$ (black curves, label 2) and $\tilde{L} = 0.1$ (blue curves, label 3) are considered. The relative weights of the radial and azimuthal components is found to strongly depend on $\tilde{L}$. Indeed $A_\mathrm{r}/A_\phi \sim 1$ at larger

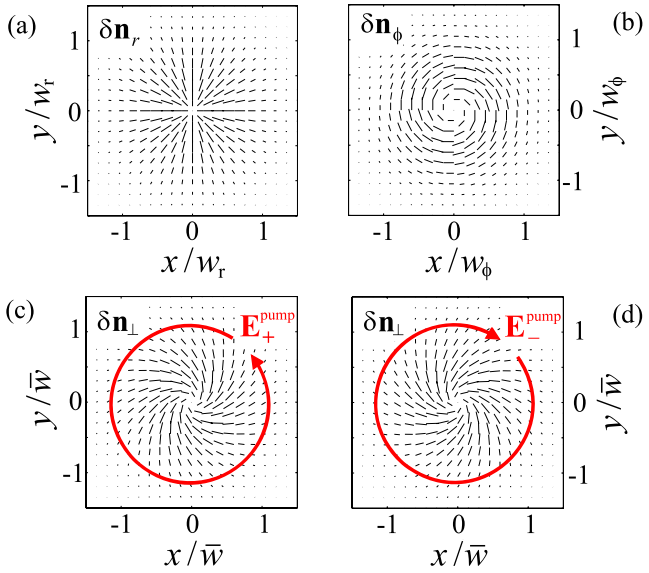

Figure 2. Light-induced radial (a), azimuthal (b) and total ((c), (d)) distorted director field pattern in the (x, y) plane, with $\bar{w} = (w_r + w_\phi)/2$. The effect of the polarization handedness of the pump beam is shown in panel (c) and (d), where the incident polarization is $\mathbf{c}_+$ and $\mathbf{c}_-$, respectively.

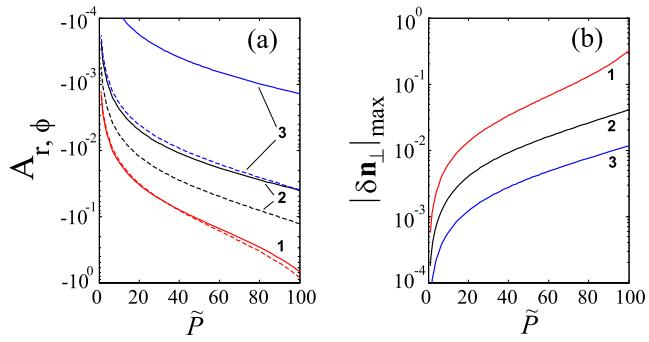

Figure 3. (a) Calculated radial (solid curves) and azimuthal (dashed curves) amplitudes A_r and A_ϕ versus power for $\tilde{L} = 10$ (red curves, label 1), $\tilde{L} = 1$ (black curves, label 2) and $\tilde{L} = 0.1$ (blue curves, label 3). (b) Maximum transverse reorientation amplitude $|\delta\mathbf{n}_\perp|_{max}$ for the same conditions as in panel (a). The incident polarization is $\mathbf{c}_+$.

$\tilde{L}$ (i.e., when the beam significantly diverges inside the liquid crystal) whereas $A_r/A_\phi \ll 1$ for smaller $\tilde{L}$ (i.e., when the beam waist is almost constant and equals w_0 throughout the film). Such a behavior can be inferred from equations ((A.6) and (A.7)). Indeed one can derive the following scaling laws: $A_r/A_\phi \propto \tilde{L}^1$ when $\tilde{L} \ll 1$ and $A_r/A_\phi \propto \tilde{L}^0$ when $\tilde{L} \gg 1$.[1] In fact these trends are clearly seen from the numerical simulations shown in figure 4(a). On the other hand, $\tilde{w}_{r,\phi}$ do not depend on power at fixed beam waist whereas they depend on the beam waist at fixed power, as shown in figure 4(b). In fact $\tilde{w}_{r,\phi}$ increase with $\tilde{L}$ and $\tilde{w}_r/\tilde{w}_\phi \lesssim 1$ in the investigated range $0.1 < \tilde{L} < 10$ (see inset of figure 4(b)).

[1] These scalings are derived in the limit of small ε by considering $w_r \sim w_\phi$, which is satisfied at least in the investigated range of $\tilde{L}$ as shown in figure 4(b).

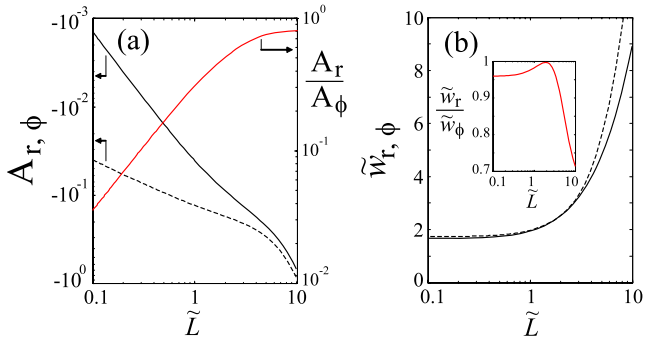

Figure 4. (a) Calculated radial (solid curves) and azimuthal (dashed curves) amplitudes A_r and A_ϕ, and ratio A_r/A_ϕ (red curve) versus $\tilde{L}$, at $\tilde{P} = 100$. (b) Reduced radial (solid curves) and azimuthal (dashed curves) waists $\tilde{w}_r$ and $\tilde{w}_\phi$ for the same conditions as in panel (a). Inset: ratio $\tilde{w}_r/\tilde{w}_\phi$. The incident polarization is $\mathbf{c}_+$.

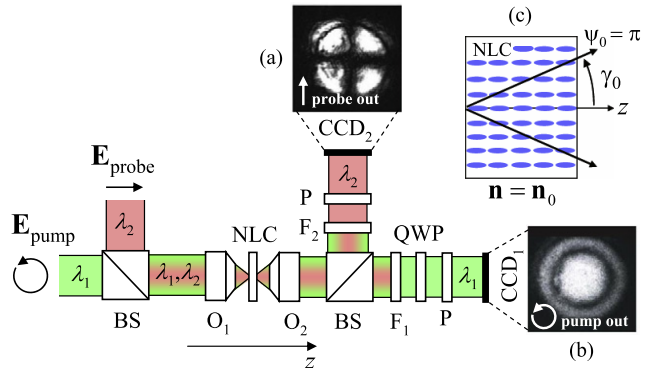

Figure 5. Experimental set-up; BS: beamsplitter; O_i: microscope objectives; NLC: nematic liquid crystal; F_i: interference filters; QWP: quarter wave plate; P: polarizer; CCD: imaging device. Panel (a) ((b)) represents the intensity distribution of the linear (circular) component of the output probe (pump) beam whose polarization state is orthogonal (parallel) to the input probe (pump) beam linear (circular) polarization when there is no significant light-induced reorientation. (c) Definition of the angle γ_0 that corresponds to a total phase delay $\psi_0 = \pi$ for the unperturbed state $\mathbf{n} = \mathbf{n}_0$, hence defining the dark ring location seen on panel (b).

3. Experiment

3.1. Set-up

The experiment is performed using the set-up shown in figure 5. A $\mathbf{c}_\pm$ polarized TEM_{00} pump beam operating at $\lambda_1 = 514.5$ nm is focused at normal incidence onto a $L = 100$ μm thick nematic liquid crystal film (E7, from Merck). Strong anchoring conditions impose $\mathbf{n} = \mathbf{n_0} = \mathbf{e}_z$ at rest. The output $\mathbf{c}_\mp$ component is extracted using a quarter wave plate and a polarization beamsplitter, and its intensity profile is visualized imaged on CCD_1 (figure 5(b)). A weak collinear linearly polarized TEM_{00} beam ($\lambda_2 = 632.8$ nm) probes the central part of the pumped region. Its output linear component whose polarization is orthogonal to the incident probe beam one is monitored on CCD_2 (figure 5(a)).

The use of an objective lens with numerical aperture NA = 0.5 in an underfilling configuration gives a beam waist

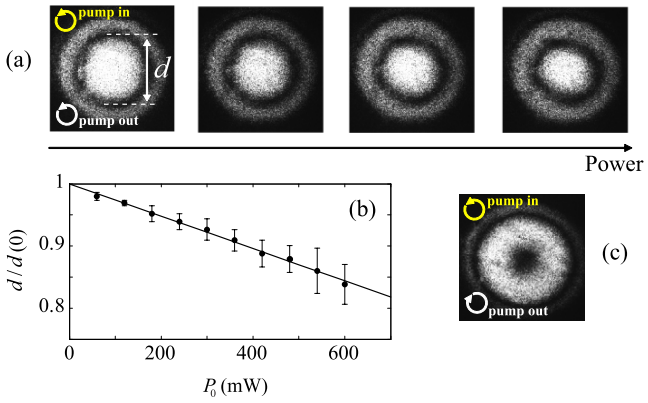

Figure 6. (a) Intensity profile of the co-polarized output circular component of the pump beam versus power. (b) Experimental power dependence of the dark ring diameter d. The solid line refers to a linear fit to guide the eyes. (c) Typical intensity profile for the contra-polarized output circular component.

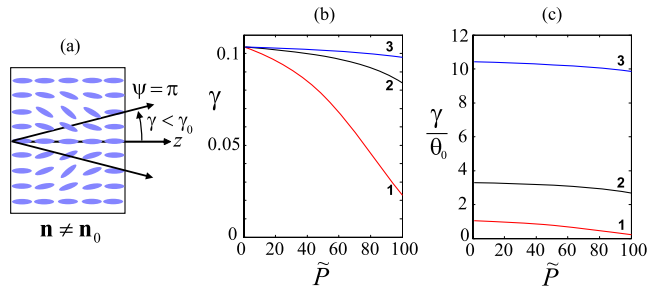

Figure 7. (a) Definition of the incidence angle γ when $\mathbf{n} \neq \mathbf{n}_0$, which corresponds to the dark ring shown in figure 6(a). (b) Calculated γ versus power for $\tilde{L} = 10$ (red curves, label 1), $\tilde{L} = 1$ (black curves, label 2) and $\tilde{L} = 0.1$ (blue curves, label 3). (c) Same as in panel (b) for the reduced angle γ/θ_0.

diameter $2w_0 \approx 2\ \mu$m and allows one to define the Rayleigh distance $z_0 \approx 10\ \mu$m from a paraxial formulation of Gaussian beams, i.e., $\tilde{L} = 10$. Hence, non-paraxial corrections to the description of the optical field (for example, see [31]) can be neglected in practice, which validates the electric field expression given by equations (8) and (9).

At low incident power, the liquid crystal is almost unperturbed and the main features expected from a c-cut uniaxial crystal are observed. Indeed we observe a Maltese cross under crossed linear polarizers, see figure 5(a), whereas a circularly symmetric intensity profile having a bell shaped envelope is observed under parallel circular polarizers, see figure 5(b). By construction, the dark ring seen in figure 5(b) thus corresponds to a polarization state that is orthogonal to the incident one. In other words it is associated with a total phase delay between extraordinary and ordinary waves $\psi_0 = \pi$ for that particular incidence angle γ_0, where the index 0 refers to the unperturbed state $\mathbf{n}_0$, as sketched in figure 5(c). Within a geometrical optics approach (note that $\tilde{L} = 10$) we have

$$\psi(\theta) = \frac{2\pi}{\lambda} n\varepsilon \int_0^L \theta^2 \, \mathrm{d}z, \tag{12}$$

where θ is the angle between a given ray of light and the optical axis (here, the z axis). We obtain

$$\gamma_0 = \theta_0 \sqrt{\frac{\pi}{2\varepsilon \tilde{L}}}, \tag{13}$$

where $\theta_0 = w_0/z_0$ is defined as the half-divergence of the beam. In the present case $\gamma_0 \sim \theta_0$, which can be qualitatively checked from figure 5(b) where the dark ring is located at the periphery of the beam (recall that θ_0 is the angle at which the intensity has decreased by e^{-2}). Also, it explains why only the first ring is visible, since higher order ones defined by the angle γ_p correspond to $\psi_p = (2p+1)\pi$, with p integer, and fall in a range where the intensity is negligible.

3.2. Light-induced radial and azimuthal reordering

Three main observations are made when the pump power is moderately increased (the strong excitation regime is addressed in section 3.3). First, the rotational invariance around the z axis of the intensity pattern recorded by CCD_1 is preserved, as shown in figure 6(a). Second, the intensity profile of the output pump beam under crossed circular polarizers is also symmetric and has a null central intensity, a typical example being shown in figure 6(c). The latter observation indicates the absence of light-induced birefringence along the z axis, $\delta\mathbf{n} = 0$ at $r = 0$, as anticipated in section 2.1, whereas the cylindrical symmetry of the output pump beam intensity on the circular polarization basis demonstrates $\partial|\delta\mathbf{n}|/\partial\phi = 0$, as expected too. Third, the dark ring diameter d decreases, hence the dark ring angle γ, as summarized in figure 6(b). The predicted trend for the power dependence of γ is obtained from the condition $\psi = \pi$ that must now take into account the inhomogeneous distribution of the local optical axis $\mathbf{n}$ along the path defined by $r = \gamma z$, as sketched in figure 7(a). For this purpose we introduce the effective angle between the considered ray of light and the local optical axis,

$$\theta_{\mathrm{eff}}(z) = \gamma + \arcsin[|\delta\mathbf{n}_\perp(r,z)|]_{r=\gamma z}, \tag{14}$$

and γ is the solution of $\psi(\theta_{\mathrm{eff}}) = \pi$. The results are summarized in figures 7(b) and (c). Unfortunately, the direct comparison with experimental data cannot be safely performed since the exact location of the pump beam is not well defined in practice.

Additional information on the light-induced elastic distortions is found from the output probe beam intensity profile collected by CCD_2. Indeed the Maltese cross is all the more twisted as the power is increased, see figure 8(a). Recalling that the main axes of a straight cross observed at rest, see figure 5(a), correspond to the input and output crossed polarizer directions for the probe beam (here, x and y), a twisted pattern reflects azimuthal distortions, $\delta n_\phi(r,z) \neq 0$, as sketched in figure 8(b). This also demonstrates a laser-induced transverse reorientation pattern with topological charge 1, in other words $\delta\mathbf{n}_\perp$ rotates by 2π over a full revolution around the z axis, as expected. We also found that the handedness of such a chiral pattern depends on the incident input polarization handedness, see figures 8(a) and (c), in agreement with expectations (see figures 2(c) and (d)).

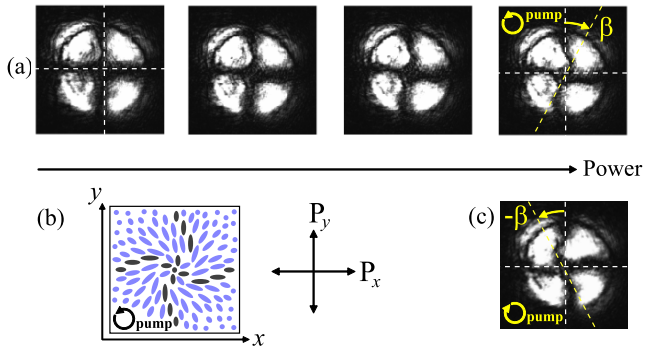

Figure 8. (a) Intensity profile of the output probe beam under crossed linear polarizers versus power. (b) Sketch of the transverse distorted director field. A circle corresponds to a liquid crystal molecule along the z axis whereas an elliptical shape refers to a molecule whose major axis is tilted with respect to z. The darkened regions correspond to the extinction directions of the polarizers $P_{x,y}$. (c) Effect of the pump beam polarization handedness on the light-induced chiral pattern handedness at fixed power. The picture should be compared to the rightmost picture of panel (a).

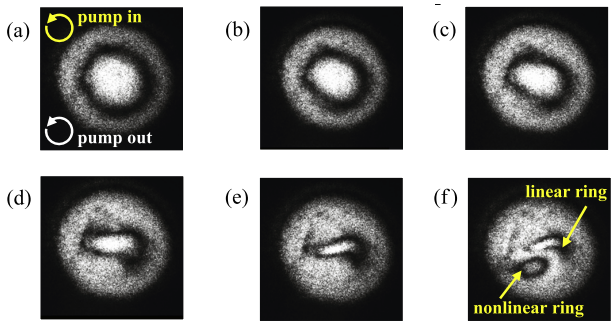

Figure 9. Illustration of the light-induced cylindrical symmetry breaking as the power is increased. Panels (a)–(f) refer to the intensity profile of the pump beam under parallel circular polarizers versus power for $P_0 \sim 600$–1200 mW in 120 mW steps. The self-focusing diffraction ring that corresponds to an off-axis hot spot of molecular reorientation is indicated in panel (f) as 'nonlinear ring' whereas 'linear ring' refers to the distorted, initially circular, dark ring.

3.3. Light-induced cylindrical symmetry breaking

As discussed in previous sections, the singular optical reordering of liquid crystals under a circularly polarized Gaussian beam involves cylindrically symmetric chiral light-induced elastic distortions (see figures 6 and 8). This strongly differs from the usual optical Fréedericksz transition under circular polarization, although the latter is also associated with light-induced chiral reorientation modes, as shown theoretically in 1990 [8] and experimentally observed ten years later [32]. Indeed, the optical Fréedericksz transition is related to spontaneous cylindrical symmetry breaking. This surprising distinction for the same interaction geometry is essentially due to the fact that 'singular' optical reordering is thresholdless whereas 'regular' reordering takes place above a threshold for the optical excitation. Consequently, in any real experiment, the optical Fréedericksz transition should be considered as an imperfect bifurcation where the bias torque (i.e., the non-zero torque exerted on the unperturbed director) preserves the cylindrical symmetry. We notice that the nature of the latter imperfect bifurcation differs from the well-known situation of the imperfect Fréedericksz transition under oblique extraordinary linear polarization [33], where the bias breaks the rotational invariance.

As a matter of fact, the beam waists that have been used so far were in the typical range $w_0 \sim 10$–100 μm in the Fréedericksz transition case, hence $\theta_0 \sim 1$–10 mrad, whereas here $w_0 \sim 1$ μm, which corresponds to $\theta_0 \sim 100$ mrad. In fact, recalling that the longitudinal field component is proportional to θ_0, this ensures a large enough amplitude for the singular torque density (see equation (1)), hence an easier observation of singular optical reordering.

Cylindrical symmetry breaking is observed for large enough power, as shown in figure 9. In particular, the chirality of the light-induced elastic distortions, which is hidden at low power when looking at the output pump beam on the circular polarization basis (see figure 6), is revealed via the broken symmetry, as illustrated in figures 9(d) and (e). Moreover, its handedness is in agreement with observations previously discussed in section 3.2 (see figure 8).

At larger power, an additional dark ring appears, as shown in figure 9(f), which is reminiscent of the optical Fréedericksz transition that is usually associated with laser-induced diffraction rings [3]. Note that the latter ring has a nonlinear nature, in contrast to the dark ring observed even at very low power, which is merely a manifestation of linear optics, as explained in section 3.1.

4. Conclusion

The concept of singular optical reordering of birefringent elastic media has been introduced and theoretically and experimentally discussed in the case of liquid crystals. In contrast to previous optical reorientation techniques, the proposed approach enables the generation of all-optically rewritable singular birefringent patterns in initially homogeneous optically anisotropic soft matter systems. This phenomenon basically relies on the spatially modulated optical dielectric torque density arising from the inherent longitudinal component of the electric field of any real beam. In practice, the singular optical patterning has been unveiled by enhancing the amplitude of the longitudinal component of the optical field owing to an appropriate focusing of the excitation light field. Cylindrically symmetric radial and spin-dependent azimuthal light-induced elastic distortion modes have been observed experimentally and a model has been derived.

Appendix A. Determination of S

The minimization of $\mathcal{F}$ within the monomodal approximation, hence with respect to $\mathbf{u} = (A_\mathrm{r}, A_\phi, w_\mathrm{r}, w_\phi)$, is derived to the first order in $A_{\mathrm{r},\phi}$. For this purpose, the elastic and optical free energy densities F_el (equation (5)) and F_opt (equation (6)) are first expanded in powers of $A_{\mathrm{r},\phi}$, then the derivatives $\partial/\partial u_k$ are performed and finally the integration along ϕ, r and z

are carried out. The calculation of the elastic contribution is straightforward and leads to

$$\frac{\partial \mathcal{F}_{\rm el}}{\partial A_{{\rm r},\phi}} = \frac{\pi K L}{32}(8 + q^2 w_{{\rm r},\phi}^2) A_{{\rm r},\phi}, \tag{A.1}$$

$$\frac{\partial \mathcal{F}_{\rm el}}{\partial w_{{\rm r},\phi}} = 0, \tag{A.2}$$

whereas the optical counterpart is more cumbersome and is derived by inserting equation (10) in equation (6) using

$$n_x = \delta n_{\rm r} \cos\phi - \delta n_\phi \sin\phi, \tag{A.3}$$

$$n_y = \delta n_{\rm r} \sin\phi + \delta n_\phi \cos\phi, \tag{A.4}$$

$$n_z \simeq 1 - (\delta n_{\rm r}^2 + \delta n_\phi^2)/2. \tag{A.5}$$

The derivatives of equation (6) with respect to $\mathbf{u}$ are then obtained and the electric field expression given by equation (8) is used. Integration along ϕ is straightforward. Integration along r benefits from the fact that the birefringence parameter ε is a small parameter [29] (i.e., only the terms up to the first order in ε are retained). Indeed, this can be done analytically since it involves Gaussian integrals of the form $\int_0^\infty r^n \exp(-Cr^2)\,{\rm d}r$, where n is an integer. The last integration, along z, has to be done numerically.

The resulting system of equations $\mathbf{S}(\mathbf{u}) = \mathbf{0}$ is, in the case of a $\mathbf{c}_+$ circularly polarized incident light beam,

$$\begin{aligned} S_1 = {} & \frac{\pi \tilde{L}}{32}(8 + \tilde{q}^2 \tilde{w}_{\rm r}^2 \theta_0^2) A_{\rm r} - 2\varepsilon \tilde{P} \int_0^{\tilde{L}} \left\{ \frac{\sin^2(\tilde{q}\tilde{z})}{1+\tilde{z}^2} \right. \\ & \times \left[\frac{A_{\rm r}}{\tilde{w}_{\rm r}^2} \left(\mathcal{I}_3^{rr} - 2\varepsilon\beta \mathcal{I}_5^{rr} - \frac{\theta_0^2}{1+\tilde{z}^2} \mathcal{I}_5^{rr} \right) + \frac{2\varepsilon\alpha A_\phi}{\tilde{w}_{\rm r}\tilde{w}_\phi} \mathcal{I}_5^{r\phi} \right] \\ & \left. + \frac{\theta_0}{\tilde{w}_{\rm r}} \frac{\sin(\tilde{q}\tilde{z})}{(1+\tilde{z}^2)^2} \left(-\tilde{z}\mathcal{I}_3^r + \varepsilon(\beta\tilde{z} - \alpha)\mathcal{I}_5^r \right) \right\} {\rm d}\tilde{z}, \end{aligned} \tag{A.6}$$

$$\begin{aligned} S_2 = {} & \frac{\pi \tilde{L}}{32}(8 + \tilde{q}^2 \tilde{w}_\phi^2 \theta_0^2) A_\phi - 2\varepsilon \tilde{P} \int_0^{\tilde{L}} \left\{ \frac{\sin^2(\tilde{q}\tilde{z})}{1+\tilde{z}^2} \right. \\ & \times \left[\frac{A_\phi}{\tilde{w}_\phi^2} \left(\mathcal{I}_3^{\phi\phi} + 2\varepsilon\beta \mathcal{I}_5^{\phi\phi} - \frac{\theta_0^2}{1+\tilde{z}^2} \mathcal{I}_5^{\phi\phi} \right) + \frac{2\varepsilon\alpha A_{\rm r}}{\tilde{w}_{\rm r}\tilde{w}_\phi} \mathcal{I}_5^{r\phi} \right] \\ & \left. - \frac{\theta_0}{\tilde{w}_\phi} \frac{\sin(\tilde{q}\tilde{z})}{(1+\tilde{z}^2)^2} \left(\mathcal{I}_3^\phi + \varepsilon(\beta + \alpha\tilde{z}) \mathcal{I}_5^\phi \right) \right\} {\rm d}\tilde{z}, \end{aligned} \tag{A.7}$$

$$\begin{aligned} S_3 = {} & \int_0^{\tilde{L}} \frac{\tilde{z}\sin(\tilde{q}\tilde{z})}{(1+\tilde{z}^2)^2} \\ & \times \left[\frac{4\tilde{z}}{\tilde{w}_{\rm r}^2} \mathcal{I}_5^r - \tilde{z}\mathcal{I}_3^r - \varepsilon(\beta\tilde{z} - \alpha) \left(\frac{4}{\tilde{w}_{\rm r}^2} \mathcal{I}_7^r - \mathcal{I}_5^r \right) \right] {\rm d}\tilde{z}, \end{aligned} \tag{A.8}$$

$$\begin{aligned} S_4 = {} & \int_0^{\tilde{L}} \frac{\sin(\tilde{q}\tilde{z})}{(1+\tilde{z}^2)^2} \\ & \times \left[\frac{4}{\tilde{w}_\phi^2} \mathcal{I}_5^\phi - \mathcal{I}_3^\phi + \varepsilon(\beta + \alpha\tilde{z}) \left(\frac{4}{\tilde{w}_\phi^2} \mathcal{I}_7^\phi - \mathcal{I}_5^\phi \right) \right] {\rm d}\tilde{z}, \end{aligned} \tag{A.9}$$

where $\theta_0 = w_0/z_0$ is defined as the half-divergence of the beam. Also, we introduced $\Delta = \varepsilon \tilde{r}^2(\alpha + {\rm i}\beta)$ with

$$\alpha(\tilde{z}) = \frac{\tilde{z}(\tilde{z}^2 - 1)}{(1+\tilde{z}^2)^2}, \tag{A.10}$$

$$\beta(\tilde{z}) = \frac{2\tilde{z}^2}{(1+\tilde{z}^2)^2}. \tag{A.11}$$

and

$$\mathcal{I}_n^a(\tilde{z}, \tilde{w}_a) = \frac{\left(\frac{n-1}{2}\right)!}{\left[2\left(\frac{1}{1+\tilde{z}^2} + \frac{1}{\tilde{w}_a^2}\right)\right]^{\frac{n+1}{2}}}, \tag{A.12}$$

$$\mathcal{I}_n^{ab}(\tilde{z}, \tilde{w}_a, \tilde{w}_b) = \frac{\left(\frac{n-1}{2}\right)!}{\left[2\left(\frac{1}{1+\tilde{z}^2} + \frac{1}{\tilde{w}_a^2} + \frac{1}{\tilde{w}_b^2}\right)\right]^{\frac{n+1}{2}}}, \tag{A.13}$$

for n odd, where $\{a, b\} = \{r, \phi\}$.

Appendix B. Approximate solution

The four-dimensional model described above is reduced to a two-dimensional one by assuming a single fixed waist for the distorted director field, $w = w_{\rm r} = w_\phi$. Such a simplification was used in [27], where $w = w_0$ was arbitrarily chosen. The latter choice, however, gets rid of the unavoidable transverse nonlocal orientational effects arising from the elasticity of the liquid crystal. The transverse nonlocal response can nevertheless be taken into account in a simple way from the dependence of the waist W of the (assumed) Gaussian reorientation profile on the pump beam waist W_0 that was derived in [34] in the case of the standard Fréedericksz optical transition. Namely, $W(W_0) = [2\sqrt{2}W_0 L/\pi]^{1/2}$. By noting that the characteristic spatial profile for the excitation field (i.e., the optical torque density) is in our case of the form $(r/w_0)\exp(-2r^2/w_0^2)$ (see section 2.1), the characteristic length associated with the Gaussian beam excitation should be taken as $W_0 = w_0/2$. Therefore we retain $w = W(w_0/2)$, which gives

$$\tilde{w} = \left[\sqrt{2} L/(\pi w_0)\right]^{1/2}. \tag{B.1}$$

The comparison between equation (B.1) and the results obtained for $\tilde{w}_{{\rm r},\phi}$ within the four-dimensional model is shown in figure B.1 for $1 < w_0 < 10\ \mu$m, which corresponds to the investigated region for $\tilde{L}$ in figure 4. A qualitative agreement is found and the corresponding approximate two-dimensional system, $\mathbf{S}'(\mathbf{u}') = \mathbf{0}$, where $\mathbf{u}' = (A_{\rm r}, A_\phi)$ is the unknown vector, is:

$$\begin{aligned} S_1' = {} & \frac{\pi \tilde{L}}{32}(8 + \tilde{q}^2 \tilde{w}^2 \theta_0^2) A_{\rm r} - 2\varepsilon \tilde{P} \int_0^{\tilde{L}} \left\{ \frac{1}{\tilde{w}^2} \frac{\sin^2(\tilde{q}\tilde{z})}{1+\tilde{z}^2} \right. \\ & \times \left[A_{\rm r} \left(\mathcal{I}_3'' - 2\varepsilon\beta \mathcal{I}_5'' - \frac{\theta_0^2}{1+\tilde{z}^2} \mathcal{I}_5'' \right) + 2\varepsilon\alpha A_\phi \mathcal{I}_5'' \right] \\ & \left. + \frac{\theta_0}{\tilde{w}} \frac{\sin(\tilde{q}\tilde{z})}{(1+\tilde{z}^2)^2} \left(-\tilde{z}\mathcal{I}_3' + \varepsilon(\beta\tilde{z} - \alpha)\mathcal{I}_5' \right) \right\} {\rm d}\tilde{z}, \end{aligned} \tag{B.2}$$

$$\begin{aligned} S_2' = {} & \frac{\pi \tilde{L}}{32}(8 + \tilde{q}^2 \tilde{w}^2 \theta_0^2) A_\phi - 2\varepsilon \tilde{P} \int_0^{\tilde{L}} \left\{ \frac{1}{\tilde{w}^2} \frac{\sin^2(\tilde{q}\tilde{z})}{1+\tilde{z}^2} \right. \\ & \times \left[A_\phi \left(\mathcal{I}_3'' + 2\varepsilon\beta \mathcal{I}_5'' - \frac{\theta_0^2}{1+\tilde{z}^2} \mathcal{I}_5'' \right) + 2\varepsilon\alpha A_{\rm r} \mathcal{I}_5'' \right] \\ & \left. - \frac{\theta_0}{\tilde{w}} \frac{\sin(\tilde{q}\tilde{z})}{(1+\tilde{z}^2)^2} (\mathcal{I}_3' + \varepsilon(\beta + \alpha\tilde{z})\mathcal{I}_5') \right\} {\rm d}\tilde{z}, \end{aligned} \tag{B.3}$$

where $\mathcal{I}_n'$ and $\mathcal{I}_n''$ refer to $\mathcal{I}_n^a$ and $\mathcal{I}_n^{ab}$, respectively, with $\tilde{w}_{\rm r} = \tilde{w}_\phi = \tilde{w}$.

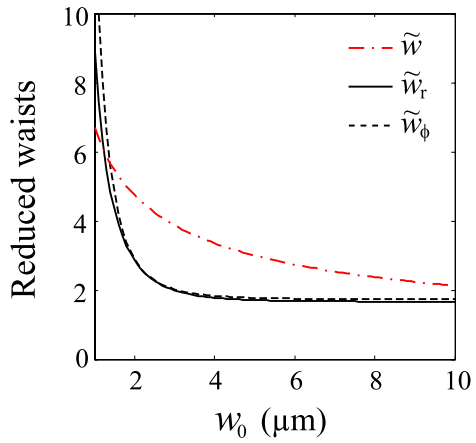

Figure B.1. Dependence on the incident beam waist w_0 of the radial (solid curve) and azimuthal (dashed curve) reduced waists, $\tilde{w}_{r,\phi}$, calculated from the four-dimensional model, and the analytical single waist approximation (dash-dotted curve), $\tilde{w}$, given by equation (B.1).

Obviously, $\mathbf{S}'(\mathbf{u}') = 0$ can be rewritten $\mathbf{m} \cdot \mathbf{u}' = \mathbf{v}$ where $\mathbf{m}$ is a 2×2 symmetric matrix and $\mathbf{v}$ is a vector, both being independent of $\mathbf{u}'$. This system admits the analytical solution

$$A_r = \frac{m_{22}v_1 - m_{12}v_2}{m_{11}m_{22} - m_{12}m_{21}}, \tag{B.4}$$

$$A_\phi = \frac{m_{11}v_2 - m_{21}v_1}{m_{11}m_{22} - m_{12}m_{21}}, \tag{B.5}$$

where m_{ij} and v_i are the elements of the matrix $\mathbf{m}$ and vector $\mathbf{v}$, respectively. Such a solution corresponds to the result derived in [27] when $\tilde{w} = 1$ but noting that the condition $n_z \equiv 1$ was there imposed in the definition of the ansatz for the distorted director field. However, although $n_z = 1$ up to the first order in the reorientation amplitude, the second order contribution (see equation (A.5)) must be taken into account when solving the problem up to the first order in $A_{r,\phi}$. Indeed, the term $\epsilon_{zz}|E_z|^2$ in the expression of the optical free energy density (see equation (6)) contributes to the final result as terms proportional to θ_0^2 in equations (B.2) and (B.3).

References

[1] Khoo I C 2009 Nonlinear optics of liquid crystalline materials *Phys. Rep.* **471** 221–67

[2] Zolot'ko A S, Kitaeva V F, Kroo N, Sobolev N N and Csillag L 1981 Light-induced Fréedericksz transition in an MBBA crystal *Pis. Zh. Eksp. Teor. Fiz.* **34** 263–7
Zolot'ko A S, Kitaeva V F, Kroo N, Sobolev N N and Csillag L 1981 *JETP Lett.* **34** 250–4 (Engl. Transl.)

[3] Durbin S D, Arakelian S M and Shen Y R 1981 Laser induced diffraction rings from a nematic liquid crystal film *Opt. Lett.* **6** 411–3

[4] Oswald P and Pieranski P 2005 *Nematic and Cholesteric Liquid Crystals: Concepts and Physical Properties Illustrated by Experiments* (London: Taylor and Francis/CRC Press)

[5] Tabiryan N V, Sukhov A V and Zel'dovich B Ya 1986 The orientational optical nonlinearity of liquid crystals *Mol. Cryst. Liq. Cryst.* **136** 1–139

[6] Santamato E, Daino B, Romagnoli M, Settembre M and Shen Y R 1986 Collective rotation of molecules driven by the angular momentum of light in a nematic film *Phys. Rev. Lett.* **57** 2423–6

[7] Santamato E, Romagnoli M, Settembre M, Daino B and Shen Y R 1988 Self-induced stimulated light scattering *Phys. Rev. Lett.* **61** 113–6

[8] Zolot'ko A S and Sukhorukov A P 1990 Fréedericksz transition induced in nematic liquid-crystal by circularly polarized-light wave *Pis. Zh. Eksp. Teor. Fiz.* **52** 707–10
Zolot'ko A S and Sukhorukov A P 1990 *JETP Lett.* **52** 62–5 (Engl. Transl.)

[9] Santamato E, Abbate G, Maddalena P, Marrucci L and Shen Y R 1990 Laser-induced nonlinear dynamics in a nematic liquid crystal film *Phys. Rev. Lett.* **64** 1377–80

[10] Marrucci L, Abbate G, Ferraiuolo S, Maddalena P and Santamato E 1992 Self-stimulated light scattering in nematic liquid crystals: theory and experiment *Phys. Rev.* A **46** 4859–68

[11] Marrucci L, Maddalena P, Arnone G, Sirleto L and Santamato E 1998 Liquid crystal reorientation induced by completely unpolarized light *Phys. Rev.* E **57** 3033–7

[12] Zolot'ko A S, Kitaeva V F, Sobolev N N, Fedorovich V Y, Sukhorukov A P, Kroo N and Csillag L 1993 Polarization dynamics of an ordinary light wave interacting with a nematic liquid crystal *Liq. Cryst.* **15** 787–97

[13] Cipparrone G, Carbone V, Versace C, Umeton C, Bartolino R and Simoni F 1993 Optically induced chaotic behavior in nematic liquid-crystal films *Phys. Rev.* E **47** 3741–4

[14] Santamato E, Maddalena P, Marrucci L and Piccirillo B 1998 Experimental study of the molecular reorientation induced by the ordinary wave in a nematic liquid crystal film *Liq. Cryst.* **25** 357–62

[15] Demeter G and Kramer L 1999 Transition to chaos via gluing bifurcations in optically excited nematic liquid crystals *Phys. Rev. Lett.* **83** 4744–7

[16] Carbone V, Cipparrone G and Russo G 2001 Homoclinic gluing bifurcations during the light induced reorientation in nematic-liquid-crystal films *Phys. Rev.* E **63** 051701

[17] Vella A, Setaro A, Piccirillo B and Santamato E 2003 On–off intermittency in chaotic rotation induced in liquid crystals by competition between spin and orbital angular momentum of light *Phys. Rev.* E **67** 051704

[18] Demeter G, Krimer D O and Kramer L 2005 Numerical study of optically induced director oscillations in nematic liquid crystals: transition to chaos via homoclinic gluings and the role of backflow *Phys. Rev.* E **72** 051712

[19] Brasselet E and Dubé L J 2006 Light-induced chaotic rotations in nematic liquid crystals *Phys. Rev.* E **73** 021704

[20] Brasselet E, Doyon B, Galstian T V and Dubé L J 2002 New laser induced spatio-temporal transition in nematics *Phys. Lett.* A **299** 212–6

[21] Brasselet E, Galstian T V, Dubé L J, Krimer D O and Kramer L 2005 Bifurcation analysis of optically induced dynamics in nematic liquid crystals: circular polarization at normal incidence *J. Opt. Soc. Am.* B **22** 1671–80

[22] Krimer D O, Kramer L, Brasselet E, Galstian T V and Dubé L J 2005 Bifurcation analysis of optically induced dynamics in nematic liquid crystals: elliptical polarization at normal incidence *J. Opt. Soc. Am.* B **22** 1681–90

[23] Krimer D O, Demeter G and Kramer L 2005 Influence of the backflow effect on the orientational dynamics induced by light in nematics *Phys. Rev.* E **71** 051711

[24] Piccirillo B, Toscano C, Vetrano F and Santamato E 2001 Orbital and spin photon angular momentum transfer in liquid crystals *Phys. Rev. Lett.* **86** 2285–8

[25] Piccirillo B, Vella A and Santamato E 2004 Optical Fréedericksz transition in liquid crystals and transfer of the orbital angular momentum of light *Phys. Rev.* E **69** 021702

[26] Brasselet E, Piccirillo B and Santamato E 2008 Three-dimensional model for light-induced chaotic rotations in liquid crystals under spin and orbital angular momentum transfer processes *Phys. Rev.* E **78** 031703
[27] Brasselet E 2009 Singular optical manipulation of birefringent elastic media using nonsingular beams *Opt. Lett.* **34** 3229–31
[28] Ciattoni A, Cincotti G and Palma C 2003 Circularly polarized beams and vortex generation in uniaxial media *J. Opt. Soc. Am.* A **20** 163–71
[29] Brasselet E, Izdebskaya Y, Shvedov V, Desyatnikov A S, Krolikowski W and Kivshar Y S 2009 Dynamics of optical spin–orbit coupling in uniaxial crystals *Opt. Lett.* **34** 1021–3
[30] Ciattoni A, Crosignani B and Di Porto P 2001 Vectorial theory of propagation in uniaxially anisotropic media *J. Opt. Soc. Am.* B **18** 1656–61
[31] Monteiro P B, Maia Neto P A and Moysés Nussenzveig H 2009 Angular momentum of focused beams: beyond the paraxial approximation *Phys. Rev.* A **79** 033830
[32] Brasselet E and Galstian T V 2001 Non-resonant light-induced chirality in non-chiral nematic liquid crystals *Opt. Commun.* **200** 241–8
[33] Durbin S D, Arakelian S M and Shen Y R 1981 Optical-field-induced birefringence and Fréedericksz transition in a nematic liquid crystal *Phys. Rev. Lett.* **47** 1411–4
[34] Zolotko A S, Kitaeva V F, Kuyumchyan V, Sobolev N, Sukhorukov A and Csillag L 1982 Light-induced second-order phase transition in a spatially bounded region of a nematic liquid crystal *Pis. Zh. Eksp. Teor. Fiz.* **36** 66–9
Zolotko A S, Kitaeva V F, Kuyumchyan V, Sobolev N, Sukhorukov A and Csillag L 1982 *JETP Lett.* **36** 80–4 (Engl. Transl.)